Quaternary Science Reviews 160 (2017) 1–12

Contents lists available at ScienceDirect

Quaternary Science Reviews

journal homepage: www.elsevier.com/locate/quascirev

Stalagmite-inferred centennial variability of the Asian summer monsoon in southwest China between 58 and 79 ka BP

Tao-Tao Zhang [a, b, c], Ting-Yong Li [a, b, c, *], Hai Cheng [d], R. Lawrence Edwards [e], Chuan-Chou Shen [f], Christoph Spötl [g], Hong-Chun Li [f], Li-Yin Han [a], Jun-Yun Li [a], Chun-Xia Huang [a], Xin Zhao [a]

[a] Chongqing Key Laboratory of Karst Environment, School of Geographical Sciences, Southwest University, Chongqing, 400715, China
[b] State Key Laboratory of Loess and Quaternary Geology, Institute of Earth Environment, Chinese Academy of Sciences, Xi'an, 710075, China
[c] Field Scientific Observation & Research Base of Karst Eco-environments at Nanchuan in Chongqing, Ministry of Land and Resources of China, Chongqing, 408435, China
[d] Institute of Global Environmental Change, Xi'an Jiaotong University, Xi'an, 710049, China
[e] Department of Earth Sciences, University of Minnesota, Minneapolis, MN, 55455, USA
[f] Department of Geosciences, National Taiwan University, Taipei, 10617, Taiwan, ROC
[g] Institut für Geologie, Universität Innsbruck, 6020 Innsbruck, Austria

ARTICLE INFO

Article history:
Received 15 July 2016
Received in revised form
27 January 2017
Accepted 1 February 2017
Available online 7 February 2017

Keywords:
Stalagmite $\delta^{18}O$
Asian summer monsoon
Greenland interstadials
Heinrich event 6
Southern Hemisphere

ABSTRACT

We use a new spliced stalagmite oxygen isotope record from Yangkou Cave and Xinya Cave, Chongqing, southwest China, to reconstruct the centennial-millennial-scale changes in Asian Summer Monsoon (ASM) intensity between 58.0 and 79.3 thousand years before present (ka BP, before AD 1950). This multidecadally resolved record shows four strong ASM periods, corresponding to Greenland Interstadials (GIS) 17–20, and three weak ASM episodes, among which, the one starting at 61.5 ± 0.2 ka BP and ending at 59.4 ± 0.2 ka BP that may correlate with Heinrich Event 6. The close agreement of climate events between China and Greenland supports the notion that the ASM is dominantly governed by high-latitude forcings in the Northern Hemisphere. The short-lived interstadial GIS 18, however, lasted for over 3 kyr in the records derived from ASM region, reflecting a gradual decline of ASM intensity, which coincides with a millennial-scale warming trend in Antarctica. This suggests an additional forcing of the ASM by the Southern Hemisphere, which also affected GIS 8–12, H4 and H5, as shown by previous speleothem studies from the ASM region.

1. Introduction

The Asian Summer Monsoon (ASM) is an integral part of the global climatic system and plays a central role in rapid climate changes involving both the Northern Hemisphere (NH) and the Southern Hemisphere (SH) (Cai et al., 2006; Barker and Knorr, 2007; Rohling et al., 2009; An et al., 2000, 2011, 2015). In recent years, the evolution of the ASM on centennial-millennial time scales since the last glacial period (LGP) has been studied using various paleoclimatic records, including stalagmites. These studies show that variability of the ASM is tightly correlated to climate changes in the northern high latitudes (e.g., Wang et al., 2001, 2005, 2008; Burns et al., 2003; Yuan et al., 2004; Shakun et al., 2007; Cosford et al., 2008; Liu et al., 2013; Duan et al., 2014, 2015; Cai et al., 2015). Other studies indicate that the ASM was also influenced by SH temperature changes during Heinrich events (H) 4 and 5 and Greenland Interstadials (GIS) 5–12 via the transequatorial flow and the migration of the position of the Intertropical Convergence Zone (ITCZ) (Cai et al., 2006; Rohling et al., 2009; Zhou et al., 2014; Han et al., 2015). High-resolution stalagmite records mainly cover Marine Isotope Stages (MIS) 1–3, while little detailed information is available on the evolution of the ASM during MIS 4. With decreasing summer insolation in the Northern Hemisphere (Berger and Loutre, 1991), increasing ice volume and sea-level lowering (Waelbroeck et al., 2002), the MIS 4 interval was an extended cold period considered to be comparable to the last glacial maximum (LGM) (North Greenland Ice Core Project

* Corresponding author. School of Geographical Sciences, Southwest University, No. 2 Tiansheng Road, Beibei district, Chongqing, 400715, China.
E-mail address: cdlty@swu.edu.cn (T.-Y. Li).

http://dx.doi.org/10.1016/j.quascirev.2017.02.003
0277-3791/

members, 2004). Therefore, a detailed study of the ASM changes during MIS 4 will improve our understanding of the progress and mechanisms of ASM evolution during the LGP and its role within the Earth climate system.

Furthermore, although GIS and H events were first identified in Greenland ice cores (Johnsen et al., 1992; Dansgaard et al., 1993) and North Atlantic sediments (Heinrich, 1988; Bond et al., 1993), their footprint has since been found throughout both hemispheres (e.g., Wang et al., 2001, 2006; Burns et al., 2003; Carolin et al., 2013; Deplazes et al., 2013; Zhou et al., 2014; Stríkis et al., 2015). Precise chronologies of GIS and H events are essential to understand their mechanisms and influences on the climate system. For marine sediments, the timing of H6 is beyond the limit of the ^{14}C dating method. And for ice cores, even the most accurate ice-core age model – the annual layer-counted GICC05 timescale – is associated with uncertainties exceeding 2.6 ka at ages >60 ka (based on 2σ maximum counting errors - Svensson et al., 2008). This lack of accurate and precise chronologies can be compensated by speleothems taking advantage of recent improvements in high-precision ^{230}Th dating (Shen et al., 2012; Cheng et al., 2013). For example, Xia et al. (2007) and Boch et al. (2011) constrained the timing of GIS using stalagmite records from Sanbao Cave, China, and the European Alps, respectively. They reported slightly younger ages for GIS 19–20 than those recorded in NGRIP. However, neither the Sanbao nor the Alps speleothems recorded the equivalents of GIS 18 and H6. Similarly, these climate events are also not registered in the seminal Hulu Cave record (Wang et al., 2001). In order to address the question whether these rapid climate events had less impact on certain regions such as China higher-resolution and precisely dated speleothem records from other caves are crucial. This is the key motivation of this study and we report here a new stalagmite record from Yangkou Cave in China, which covers the entire MIS 4 interval. High U concentrations resulted in age uncertainties of less than 0.5% (Li et al., 2014a; Han et al., 2016) allowing to accurately reconstruct the evolution of ASM during MIS 4 and to assess potential forcing mechanisms.

2. Cave site and stalagmite sample

Stalagmite JFYK7 was collected in Yangkou Cave (29°02′N, 107°11′E, 2140 m a.s.l.) (Fig. 1), which is located in Jinfo Mountain, Chongqing City, southwest China. The study site is situated at the northern border region between the Sichuan Basin and the Yun-Gui Plateau. The cave is 2245 m in length and developed in Permian limestones. The climate in this region is mainly controlled by the Asian monsoon. The mean annual temperature and precipitation are about 8.5 °C and 1400 mm, respectively. About 83% of the rain falls in the rainy season between April and October (Zhang et al., 1998).

Stalagmite JFYK7 is approximately 125 mm and 40 mm wide at the bottom and top, respectively. It is composed of dark brown calcite and its the internal structure reveals a clear submillimeter-scale layering (Fig. 2 in Han et al., 2016). The length of the growth axis, which changed its orientation during the growth history, is 555 mm. With the exception of a clear hiatus between 452.5 and 453 mm distance from top the stalagmite shows no macroscopic evidence of further growth interruptions.

In this study, we present data from the section between 367 mm and 555 mm distance from the top, which covers MIS 4.

3. Methods

3.1. U-Th dating

Sixteen sub-samples were ^{230}Th-dated. Approximately 80 mg of calcite powder was drilled along individual growth layers using a 1-mm carbide dental drill. Procedures for chemical separation and purification of U and Th are described in Shen et al. (2003, 2012). Dating was performed at the University of Minnesota, USA, and the Xi'an Jiaotong University, China. A Thermo Fisher Neptune multi-collector inductively coupled plasma mass spectrometer (MC-ICP-MS) with a secondary electron multiplier was used for the determination of the U-Th isotopic contents and compositions (Shen et al., 2012; Cheng et al., 2013). The decay constants of ^{230}Th, ^{234}U, and ^{238}U are 9.1705×10^{-6} yr^{-1}, $2.82{,}206 \times 10^{-6}$ yr^{-1} (Cheng et al., 2013), and $1.55{,}125 \times 10^{-10}$ yr^{-1} (Jaffey et al., 1971),

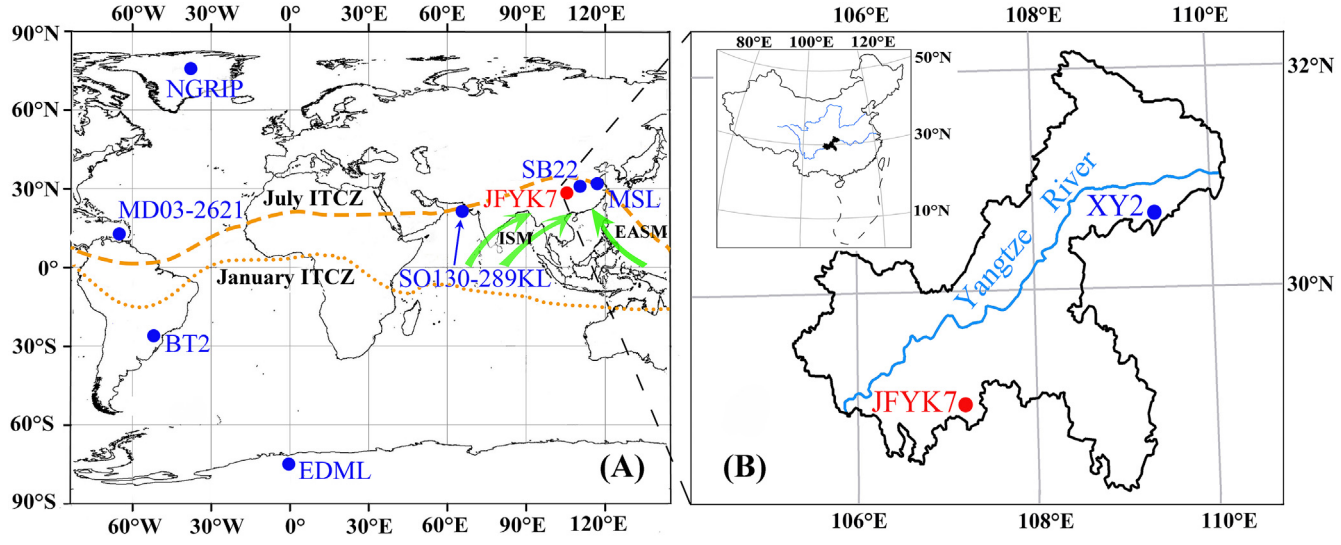

Fig. 1. (A) Location of Yangkou cave (stalagmite JFYK7, red dot) and other paleoclimatic records (blue dots): MSL (Hulu Cave; Wang et al., 2001), SB22 (Sanbao Cave; Wang et al., 2008), SO130-289KL (northeastern Arabian Sea), MD03-2621 (Cariaco Basin, Deplazes et al., 2013), BT2 (Botuverá Cave, Cruz et al., 2005), NGRIP (North Greenland Ice Core Project members, 2004), and EDML (EPICA Community Members., 2006). Green arrows depict the present-day surface wind directions of the ISM and EASM. (B) Chongqing City and the locations of Yangkou cave (stalagmite JFYK7, red dot) and Xinya Cave (stalagmite XY2, blue dot). (For interpretation of the references to colour in this figure legend, the reader is referred to the web version of this article.)

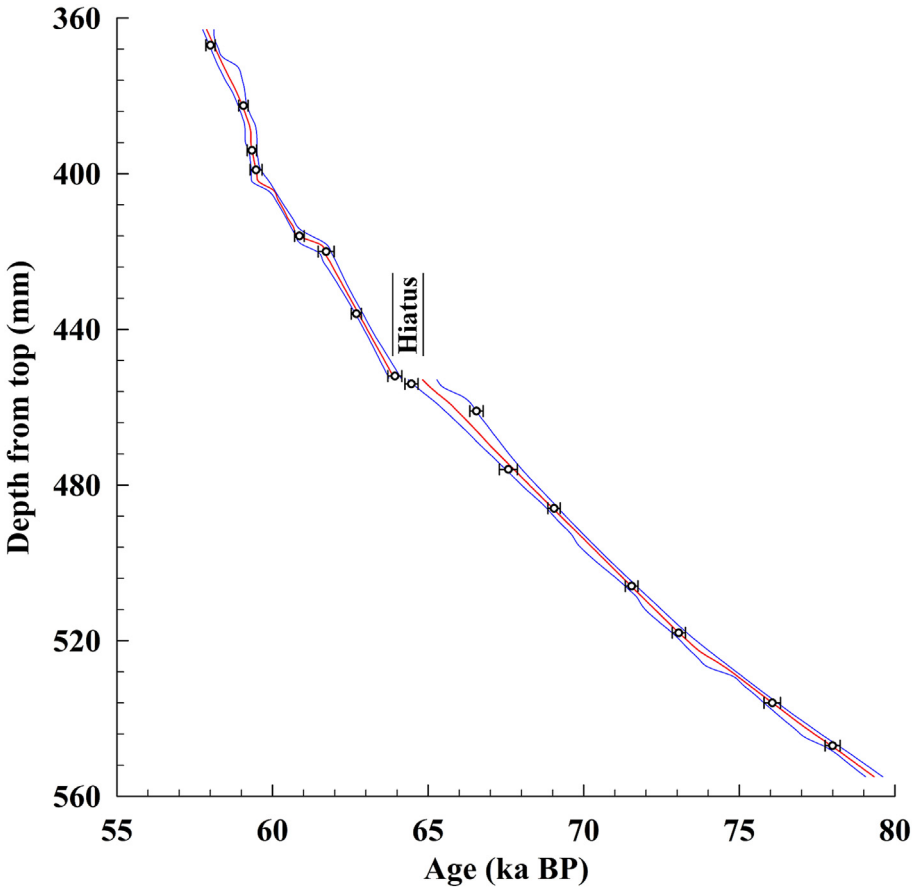

Fig. 2. Age model of stalagmite JFYK7. ^{230}Th dates are shown with their 2σ uncertainties. StalAge was used to build the age model (Scholz and Hoffmann, 2011). The blue lines denote the upper and lower 95%-confidence limits. (For interpretation of the references to colour in this figure legend, the reader is referred to the web version of this article.)

respectively. The age correction for the initial ^{230}Th was performed using the average crustal ^{230}Th/^{232}Th ratio of 4.4 ± 2.2 × 10^{-6} (Taylor and McLennan, 1995).

3.2. Oxygen isotope analyses

A total of 386 sub-samples were drilled for stable isotope analysis along the growth axis at 0.5 mm intervals using a 0.5 mm carbide dental drill, resulting in a mean resolution of ~45 years. Analyses were performed on a Delta V Plus isotope ratio mass spectrometer equipped with a Kiel IV Carbonate Device at the Geochemistry and Isotope Laboratory of Southwest University, China. Isotopic results are given with respect to the Vienna Pee Dee Belemnite (V-PDB) standard with a one-sigma external error < ±0.1‰ for δ^{18}O and < ±0.06‰ for δ^{13}C (Li et al., 2011).

3.3. Test of equilibrium deposition

As a first step, the Hendy test (Hendy, 1971) was applied to evaluate whether calcite was deposited under isotopic equilibrium conditions. We drilled 28 sub-samples from four distinct growth layers. The analytical method is described in section 3.2. For each layer, the variability of δ^{18}O values was less than 0.5‰, and there is no progressive increase in δ^{18}O values from the center towards the flanks (Fig. 3A). Furthermore, there is no apparent correlation between δ^{18}O and δ^{13}C for any of the layers (Fig. 3B). These observations suggest that stalagmite JFYK7 satisfies the Hendy test.

The replication of paleoclimate records, however, is a more robust test for evaluating the likelihood of calcite deposition under isotopic equilibrium conditions (cf. Dorale and Liu, 2009). Both Yangkou Cave (stalagmite JFYK7) and Xinya Cave (stalagmite XY2 - Li et al., 2007) are located in Chongqing and are approximately 280 km apart. Despite different bedrock, soil, and vegetation, both sites are controlled by the same ASM climate system (Fig. 1). During the overlapping interval between 58.0 and 63.9 ka BP (Fig. 4) the δ^{18}O patterns of the two stalagmites agree within age uncertainties. Therefore, the JFYK7 record also satisfies the replication test. These two tests strongly suggest that there was negligible kinetic isotopic fractionation during the deposition of stalagmite JFYK7. Hence, the δ^{18}O signals recorded in JFYK7 primarily reflect climate.

4. Results

4.1. Age model

All dates are in stratigraphic order and U and Th isotopic compositions and ^{230}Th dates are given in Table 1. ^{238}U and ^{232}Th concentrations range from 5.7 to 14.0 ppm and from 0.16 to 1.5 ppb, respectively. The high ^{238}U content and the high ^{230}Th/^{232}Th ratio of 26,220–634,477 (ppm) yielded high-precision dates with uncertainties of less than 0.4%. There is a 900 yr hiatus between 452.5 and 453 mm distance from top. A probabilistic Monte Carlo approach method (Scholz and Hoffmann, 2011) was used to establish a depth-age model of stalagmite JFYK7 (Fig. 2).

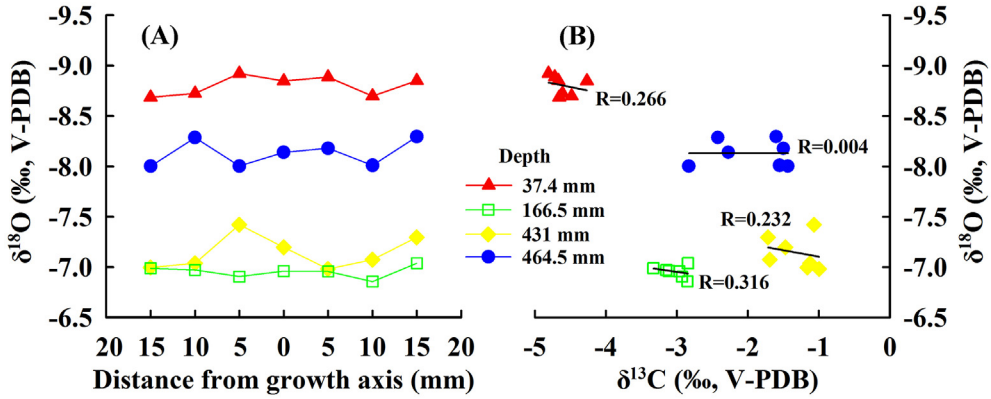

Fig. 3. Hendy tests of stalagmite JFYK7. (A) $\delta^{18}O$ values of four growth layers. (B) $\delta^{18}O$ versus $\delta^{13}C$ for coeval subsamples.

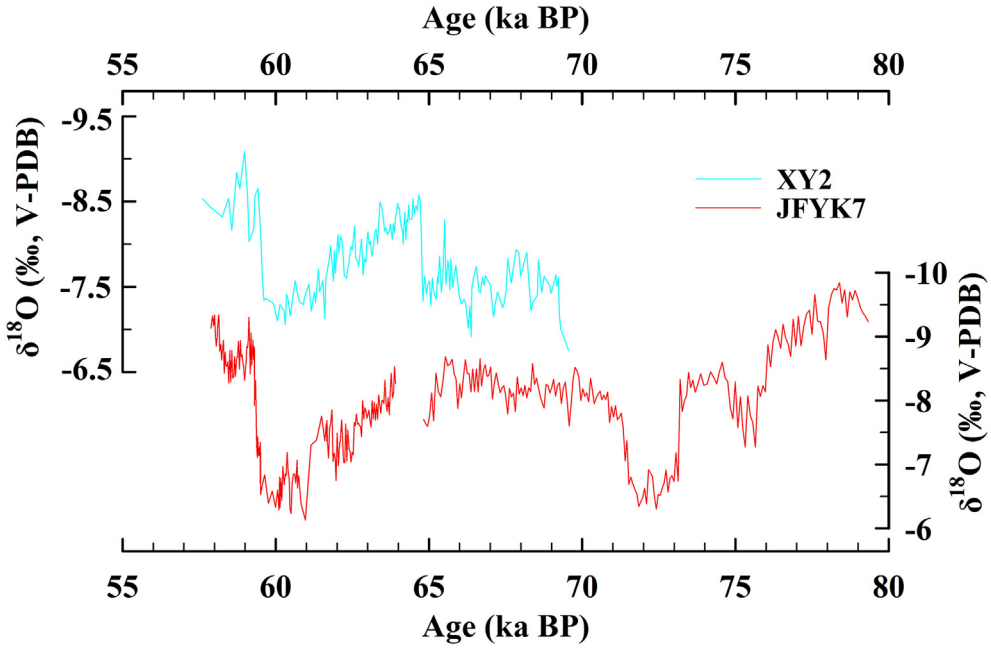

Fig. 4. $\delta^{18}O$ records of stalagmites JFYK7 and XY2 (Li et al., 2007).

4.2. Oxygen isotope composition

The $\delta^{18}O$ values show large shifts along the growth axis, ranging from −9.8 to −6.1‰, with an average of −8.0‰ (Fig. 4). There is a hiatus between 63.9 and 64.8 ka BP, which corresponds to the macroscopic boundary between 452.5 and 453 mm distance from top. Multiple factors that can lead to a growth stop in speleothems. These include climate change, e.g. a prolonged drought, and processes related to changes in the karst system, such as the blocking and/or change of seepage routes. A transition towards drier conditions leading to a growth stop is typically associated with sharply increasing oxygen and in particular carbon isotope values. As no such trend is observed in JFYK7 (Fig. 4), the hiatus between 63.9 and 64.8 ka BP is attributed to site-specific factors. Fortunately, stalagmite XY2 from Xinya Cave, also located in Chongqing City (Fig. 1b), recorded the interval from 57.6 to 69.5 ka BP (Li et al., 2007) (Fig. 4). Using this record, we obtained a complete $\delta^{18}O$ sequence covering the interval from 57.6 to 79.3 ka BP (Fig. 4).

Between 79.3 and 71.2 ka BP the $\delta^{18}O$ values gradually increase from −9.8‰ to −7.8‰ and are punctuated by two abrupt events at 76.0–74.7 ka BP and 73.2–71.2 ka BP, with a sudden increase of 1.6‰ and 2.0‰, respectively. Between 71.2 and 64.8 ka BP $\delta^{18}O$ values maintain rather stable and low, followed by rapid decrease by 1.2‰ at ~64.8 ka BP (Li et al., 2007). $\delta^{18}O$ slowly increased afterwards between 64.7 and 60.0 ka BP, followed again by a marked decrease (Fig. 4).

5. Discussion

5.1. $\delta^{18}O$ interpretation

Under isotopic equilibrium conditions, stalagmite $\delta^{18}O$ variability is controlled by the cave temperature (−0.23‰/°C, O'Neil et al., 1969) and the isotopic composition of drip water which is a function of the annual weighted mean $\delta^{18}O$ value of meteoric precipitation. Caley et al. (2014) argued that in South Asian, encompassing Sanbao, Hulu, and Dongge cave sites, the air temperature over the last 150,000 years varied by about 3 °C only. For caves such as Yangkou cave with tens to hundreds of meters of rock

Table 1
^{230}Th dating results of stalagmite JFYK7.

Sample ID	Depth (mm)	^{238}U (ppb)	^{232}Th (ppt)	δ^{234}U measured	^{230}Th/^{238}U activity	^{230}Th/^{232}Th (ppm)	^{230}Th age (a) uncorrected	^{230}Th age (a BP) corrected	$\delta^{234}U_{initial}$ corrected
JFYK7-1520	367	6933 ± 6.5	328 ± 9	27.5 ± 1.3	0.4252 ± 0.0006	148,372 ± 4233	58,072 ± 149	58,007 ± 149	32 ± 2
JFYK7-1521	382.5	9240 ± 8.7	191 ± 7	6.3 ± 1.3	0.4214 ± 0.0006	335,513 ± 11,756	59,127 ± 151	59,063 ± 151	7 ± 2
JFYK7-1522	394	13,984 ± 14.2	156 ± 7	18.8 ± 1.3	0.4285 ± 0.0006	634,477 ± 28,407	59,401 ± 149	59,336 ± 149	22 ± 2
JFYK7-16	399	13,763 ± 15.8	222 ± 16	17.8 ± 1.7	0.4288 ± 0.0007	438,464 ± 31,977	59,531 ± 191	59,469 ± 191	21 ± 2
JFYK7-1523	416	10,298 ± 11	424 ± 11	−4.1 ± 1.2	0.4262 ± 0.0006	170,508 ± 4366	60,927 ± 156	60,862 ± 156	−5±1
JFYK7-17	420	10,026 ± 12.8	243 ± 11	1.2 ± 2.4	0.4331 ± 0.0007	294,121 ± 13,372	61,784 ± 256	61,721 ± 256	1 ± 3
JFYK7-1524	436	11,257 ± 11.4	387 ± 9	−11.1 ± 1.3	0.4323 ± 0.0006	207,310 ± 5016	62,759 ± 164	62,694 ± 164	−13 ± 2
JFYK7-18	452	13,287 ± 16.7	178 ± 19	−11.0 ± 1.8	0.4386 ± 0.0007	540,334 ± 58,103	63,994 ± 225	63,931 ± 225	−13 ± 2
JFYK-7-S1	454	5673.8 ± 6.4	1536 ± 37	−33.5 ± 1.2	0.4304 ± 0.0008	26,220 ± 625	64,537 ± 210	64,529 ± 210	−40 ± 1
JFYK-7-S2	461	10,975.6 ± 14.5	141 ± 22	−0.4 ± 1.2	0.4570 ± 0.0009	585,457 ± 90,089	66,618 ± 214	66,618 ± 214	0 ± 1
JFYK-7-S3	476	10,775.8 ± 22.2	138 ± 19	−37.3 ± 1.7	0.4434 ± 0.0011	571,767 ± 78,759	67,642 ± 289	67,642 ± 289	−45 ± 1
JFYK7-1525	486	10,308.5 ± 11.6	263 ± 8	−22.1 ± 1.3	0.4581 ± 0.0007	296,537 ± 9310	69,113 ± 199	69,048 ± 199	−27 ± 2
JFYK7-1526	506	7622.2 ± 7.2	871 ± 19	−25.1 ± 1.3	0.4682 ± 0.0006	67,547 ± 1457	71,607 ± 202	71,540 ± 202	−31 ± 2
JFYK7-1527	518	8984.0 ± 8.7	228 ± 8	−46.5 ± 1.3	0.4636 ± 0.0006	301,001 ± 10,412	73,118 ± 212	73,053 ± 212	−57 ± 2
JFYK7-20	536	9388.5 ± 11.5	528 ± 11	−60.1 ± 1.5	0.4692 ± 0.0008	137,566 ± 2810	76,119 ± 266	76,058 ± 266	−74 ± 2
JFYK7-1528	547	9688.2 ± 10.9	261 ± 8	−67.0 ± 1.3	0.4743 ± 0.0007	289,825 ± 8940	78,060 ± 240	77,995 ± 240	−84 ± 2

$\lambda^{230} = 9.1705 \times 10^{-6}\ Y^{-1}$; $\lambda^{234} = 2.82{,}205 \times 10^{-6}\ Y^{-1}$; $\lambda^{238} = 1.55{,}125 \times 10^{-10}\ Y^{-1}$.
$\delta^{234}U = ([^{234}U/^{238}U]^{-1}_{activity}) \times 1000$. $\delta^{234}U_{initial}$ was calculated based on ^{230}Th age (T), i.e., $\delta^{234}U_{initial} = \delta^{234}U_{measured} \times e^{\lambda 234 \times T}$.
Corrected ^{230}Th ages assume an initial ^{230}Th/^{232}Th atomic ratio of $4.4 \pm 2.2 \times 10^{-6}$.
These are the values for a material at secular equilibrium, with a bulk earth ^{232}Th/^{238}U value of 3.8. The errors are arbitrarily assumed to be 50%.
B.P. stands for "Before Present", where "Present" is defined as the year 1950 A.D.
Sub-samples JFYK7-16, JFYK7-17, JFYK7-18, and JFYK7-20 were dated at University of Minnesota, USA, and the others were dated at Xi'an Jiaotong University, China.

overburden, the cave air temperature is very close to the average air temperature outside the cave. So, this magnitude of temperature change (3 °C) can only account for a maximum of 0.7‰ of the speleothem calcite $\delta^{18}O$ signal. Considering that the amplitude of $\delta^{18}O$ variation in stalagmite JFYK7 reaches 3.7‰, the dominant control on stalagmite $\delta^{18}O$ is not cave temperature but the drip water oxygen isotopic composition. Data from local meteoric precipitation and multi-annual monitoring of drip sites in Yangkou cave showed that there is insignificant evaporation prior to infiltration (Wang et al., 2014a). The intra-annual variation of drip water $\delta^{18}O$ follows the seasonal cycle $\delta^{18}O$ of rainfall, albeit with a much reduced amplitude due the groundwater mixing, and hence reflects the average $\delta^{18}O$ of the local precipitation (Wang et al., 2014a).

The ASM includes the Indian Summer Monsoon (ISM) and the East Asian Summer monsoon (EASM) (Wang and Lin, 2002; Ding and Chan, 2005; Li et al., 2014b; Liu et al., 2015). In the ISM regions, precipitation originates from a single water vapor source (the Indian Ocean), and the $\delta^{18}O$ value of meteoric precipitation is inversely correlated to the rainfall amount. $\delta^{18}O$ values of stalagmites from the ISM realm have therefore been regarded as a proxy for the intensity of the ISM (Neff et al., 2001; Fleitmann et al., 2003, 2007; Sinha et al., 2005; Shakun et al., 2007). The variability of the EASM rainfall is more complex and can be attributed to several factors (Sun et al., 2009; references therein; Liu et al., 2015). Hence, the climate significance of stalagmite $\delta^{18}O$ data from this region remains controversial. Traditionally, stalagmite $\delta^{18}O$ records from eastern China have been interpreted as a proxy of EASM intensity or summer rainfall amount (Wang et al., 2001, 2005; Cheng et al., 2009). This interpretation, however, has been challenged recently (e.g. Dayem et al., 2010; Pausata et al., 2011; Liu et al., 2014).

Modern meteorological studies indicate that the EASM is composed of the South China Sea tropical monsoon (part of the ITCZ) and the subtropical monsoon which are antiphase with each other (Tao and Chen, 1987; He et al., 2008; Tan, 2009). These observations also demonstrate that the rainfall in the northern China is negatively correlated with that in southern China, especially in the middle and lower reaches of the Yangtze River (Zhao and Zhou, 2006; Ding et al., 2008). Interestingly, however, the stalagmite $\delta^{18}O$ records from these regions are similar (Tan, 2009). According to modern observations, the bulk of the moisture for summer precipitation over the EASM region is derived from the Indian Ocean (Ding et al., 2004, 2008; Tian et al., 2004; Drumond et al., 2011; Cheng et al., 2012). Cheng et al. (2012) suggested that the stalagmite $\delta^{18}O$ records from EASM region reflect a mean state of summer monsoon intensity or integrated moisture transport rather than the amount of local precipitation.

Tan (2009, 2011 and 2014) pointed out that the relaxation of the trade winds controls major changes in stalagmite $\delta^{18}O$ from the EASM region. When the ISM intensifies, rainfall over the ISM regions increases. In the EASM region, an increase in water vapor from the southern Indian Ocean will result in lower $\delta^{18}O$ values of precipitation, eventually recorded in stalagmites, but the rainfall amount in EASM regions does not necessarily increase (Tan, 2009, 2011). In other words, the lower $\delta^{18}O$ values of precipitation mainly reflect a change of moisture source rather than of rainfall amount. Most recently, Liu et al. (2015) also argued that stalagmite $\delta^{18}O$ records from the EASM region mainly reflect changes in ISM intensity.

We therefore interpret the Yangkou stalagmite $\delta^{18}O$ record as a potential proxy of the ISM intensity on centennial to millennial time scales, whereby more negative $\delta^{18}O$ values reflect an intensified ISM and vice versa.

5.2. Comparison between the ASM and global climate

Although the millennial-scale variability of the ASM recorded by stalagmites JFYK7 and XY2 is not entirely consistent with the change in summer insolation at 30 °N between 79.3 and 58.0 ka BP (Fig. 5B), we suggest that the variability of the ASM is regulated by the summer insolation on orbital timescale (Wang et al., 2001, 2014b).

A series of millennial-scale climatic fluctuations are superimposed on the first-order trend, which may correlate to temperature changes recorded in Greenland ice cores (Fig. 5A and B). The $\delta^{18}O$ sequence of JFYK7 records at least four strong ASM events, indicated by negative $\delta^{18}O$ excursions, which correspond to GIS 17–20 (Fig. 5A and B). In addition, three positive excursions

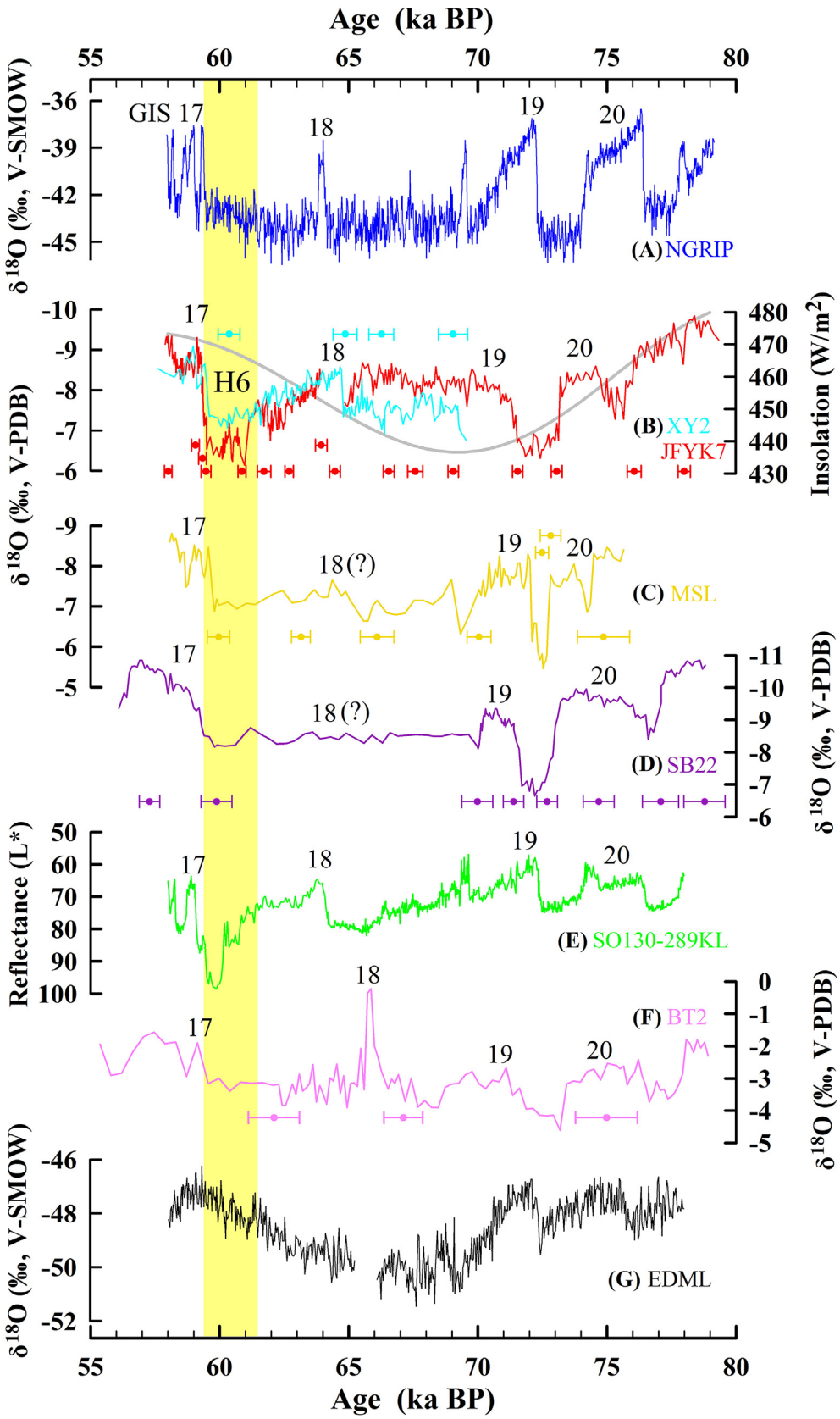

Fig. 5. Comparison of the JFYK7 record with other paleoclimatic records. GIS events 17–20 are marked in Arabic numerals for each record. (A) NGRIP (North Greenland Ice Core Project members, 2004). (B) $\delta^{18}O$ profiles of stalagmites JFYK7 (red) and XY2 (cyan) (Li et al., 2007); the gray curve shows the 30°N summer insolation (Berger and Loutre, 1991). (C) Stalagmite records MSL from Hulu Cave (Wang et al., 2001) and (D) SB22 from Sanbao Cave (Wang et al., 2008). (E) Total reflectance profile of northeastern Arabian Sea sediment core SO130-289KL (100-points running mean) (Deplazes et al., 2013). (F) Stalagmite BT2 from Brazil (Cruz et al., 2005), note inverted scale. (G) Antarctic EDML ice core (EPICA Community Members., 2006). ^{230}Th dates and associated uncertainties ($\pm 2\sigma$) are shown for all stalagmite records. The yellow vertical bar marks the expression of H6 in the different records. (For interpretation of the references to colour in this figure legend, the reader is referred to the web version of this article.)

occurred at 76.0–74.7, 73.2–71.2, and 61.5–59.4 ka BP, reflecting weak ASM events, and their counterparts can also be found in the NGRIP records (Fig. 5A and B). Finally, the weak ASM event at 61.5–59.4 ka BP may correspond to Heinrich event 6 (Heinrich, 1988).

There is a notable exception, however. The interval between 69.6 and 64.8 ka BP, which corresponds to cold conditions in Greenland, is characterized by negative $\delta^{18}O$ values in the JFYK7 record, suggesting rather intense monsoon conditions. Other speleothem records from the ASM region also show moderately low $\delta^{18}O$ values during this time interval of MIS 4 (Fig. 5A and B). This apparent mismatch between climate change in Greenland and the ASM region may result from at least two factors. Firstly, cold conditions in Antarctica may have intensified the transequatorial air flow (Fig. 5G) leading to a strong ASM (An et al., 2000; 2011; Xue et al., 2004; Cai et al., 2006). Secondly, during this period, sea level was ~80 m lower than today (Waelbroeck et al., 2002), exposing the continental shelf around the Gulf of Thailand and the South China Sea, where evaporation was reduced and stratiform precipitation increased, contributing to depleted $\delta^{18}O$ values of the water vapor and hence lower precipitation $\delta^{18}O$ values in the study area (Li et al., 2014a,b; Cai et al., 2015).

At millennial timescales, the variability of the ASM was tightly coupled to climate change in the northern high latitudes during our study period. Various mechanisms have been discussed that link the evolution of the ASM and climate change in the NH. Some studies suggest that air temperature changes over the North Atlantic and Greenland are transferred to Siberia by the westerlies, where they affect the strength of the Siberian high-pressure cell that regulates the intensity of the Asian winter monsoon (AWM) (Porter and An, 1995; Sun et al., 2012).

In general, weaker winter monsoons are correlated with stronger summer monsoons, and vice versa (Ding et al., 1995; Sagawa et al., 2014). But some researchers considered that the relationship between ASM and AWM was not necessarily reversed during certain periods (Zhang and Lu, 2007; Steinke et al., 2011). In addition to the westerlies, North Atlantic Deep Water (NADW) formation as part of the thermohaline circulation may result in changes in sea-surface temperatures (SST) in the tropical western Pacific (Sirocko, 2003; Alley, 2005), which induce the movement of the West Pacific Tropical High (WPTH), influencing the intensity of the EASM (Wang and Chen, 2012). In addition, the migration of the mean position of the ITCZ can, to some extent, also link climate change in the NH to the variability of the ASM (Chiang et al., 2003; Chiang and Bitz, 2005). At present, it is unclear which of these mechanisms was dominant during MIS 4. Denser networks of high-precision paleoclimate records in conjunction with climate simulations are essential to address this important question.

Furthermore, the variability of the ASM may be influenced by some other factors. For example, the weak monsoon event between 73.2 and 71.2 ka BP is possibly related to the Toba eruption which is the largest mega-eruption during the Quaternary, and occurred at the very beginning of the stadial following GIS 20 (Ninkovich et al., 1978; Zielinski et al., 1996; Storey et al., 2012). Huge volumes of sulphur injected into the stratosphere during this eruption was oxidised to form sulphate aerosols that decreased the amount of solar radiation reaching the surface and led to a cooling (Self, 2006). Rampino and Self (1992, 1993) suggested a regional to possibly hemispheric cooling of 3–5 °C following the Toba eruption. Data from the GISP2 ice core from Greenland record a cooling that lasted several centuries following this eruption (Zielinski et al., 1996). In general, cooler temperatures decrease the land-sea thermal contrast and subsequently weaken the ASM. A marine core from the Bay of Bengal indicates initially cooler temperatures followed by decreasing tree cover and prolonged drought for at least a millennium in the south Asia following the Toba eruption (Williams et al., 2009). In addition, a climate simulation also showed that precipitation in India and Southeast Asia was reduced after the eruption (Timmreck et al., 2012). We note, however, that the stadial between GIS 20 and 19 started prior to the eruption (Zielinski et al., 1996). Schulz et al. (2002) suggested that Toba had only a minor impact on the evolution of ISM on centennial to millennial time scales. And a model research shows that following the eruption, there was an extreme initial cooling, which, however, was limited to no more than about one or two decades (Robock et al., 2009). Therefore, we cautiously consider that the Toba mega-eruption might have acted as an “accelerator” or “enhancer” rather than a “trigger” for the evolution of the weak ASM event following GIS 20. The other weak ASM event between 76 and 75 ka BP occurred before GIS 20, i.e. it occurred prior the Toba eruption. If this weak ASM event was associated with another volcano eruption is unknown.

Currently available speleothem records from southern China – stalagmites MSL and SB22 from Hulu Cave and Sanbao Cave, respectively – show broad agreement with the pattern of millennial-scale ASM variability as reported in this study (Wang et al., 2001, 2008 - Fig. 5B–D), suggesting that the climate over the Chinese monsoon regions varied synchronously on millennial time scale during MIS 4, although both instrumental and some paleoclimatic records exhibit significant spatial variations in rainfall on decadal-centennial time scales over eastern China (Liu et al., 2015 and therein). However, there are some small-scale differences with regard to the structure and timing of each abrupt climate event recorded in JFYK7, MSL and SB22. These minor differences reflect different temporal resolutions and levels of dating precision. For example, the $\delta^{18}O$ resolution of stalagmites MSL and SB22 is ~200 years, and their age models are based on only seven and eight ^{230}Th dates, respectively. In contrast, the $\delta^{18}O$ resolution of JFYK7 is ~45 years, and the age model is constrained by sixteen higher-precision dates (Fig. 5B–D). In addition, site-specific parameters, such as the local climate, geology and/or hydrology, may also in part influence the speleothem $\delta^{18}O$ records (cf. Fairchild et al., 2006). More high-resolution and high-precision stalagmite records are therefore needed to establish the detailed evolution of the ASM during MIS 4.

The evolution of the ISM as one of the key components of the ASM system was previously reconstructed based on the change in total reflectance of marine sediments from site SO130-289KL in the northeastern Arabian Sea (Deplazes et al., 2013 - Fig. 1A). During MIS 4, there are four strong ISM events corresponding to GIS 17–20. In addition, a markedly weak ISM event occurred at ~60 ka BP that may correlate to H6 event (Fig. 5E, Deplazes et al., 2013). The reflectance pattern of marine sediments from Arabian Sea agrees well with the stalagmite record JFYK7 within age uncertainties (Fig. 5B and E). However, there are minor differences between SO130-289KL and stalagmite records MSL and SB22 (Wang et al., 2001, 2008 - Fig. 5C–E). For example, equivalents of GIS 18 and H6 are recorded both by $\delta^{18}O$ shifts in stalagmites JFYK7 and XY2 and by reflectance data of core SO130-289KL (Fig. 5B and E). In contrast, stalagmites SB22 and MSL lack clear expressions of GIS 18 and H6, partly because of a low-resolution chronology between 58 and 79 ka BP (Fig. 5C and D). As a whole, despite of these minor differences, the variability of the ISM is consistent with the EASM on millennial time scales during MIS 4 (Fig. 5B–E). This consistency suggests that the ISM and the EASM are regulated by climate change over the northern high latitudes (Wang et al., 2001; Broccoli et al., 2006; Deplazes et al., 2014), and the moisture from the Indian Ocean not only dominates the precipitation in the ISM region but also the transport to the EASM area (Ding et al., 2004, 2008; Tian et al., 2004; Drumond et al., 2011; Cheng et al., 2012).

Comparing the $\delta^{18}O$ records of stalagmite JFYK7 and stalagmite BT2 from southeast Brazil (Fig. 1A) reveals a prominent anti-phase relationship at millennial timescales between the ASM and the South American Summer Monsoon (SASM) (Fig. 5B and F), reflecting the migration of the ITCZ and the asymmetry of the Hadley circulation in the two hemispheres (Wang et al., 2006, 2007). As a result of ice-sheet growth in the high latitudes of the NH, the Atlantic Meridional Overturning Circulation (AMOC) declined and resulted in the southward migration of the ITCZ, giving rise to higher SSTs in the subtropical South Atlantic Ocean and a strengthening of the SASM (Broecker, 1998; Chiang et al., 2003; Wang et al., 2006). In the NH, the intensities of the ISM and the EASM decreased as a consequence of this southward migration of the ITCZ. Finally, this also strengthened the updraft/downdraft flow of the Hadley circulation in the SH/NH and resulted in an increase/decrease of rainfall in the low latitudes of the SH/NH (Clement et al., 2004; Broccoli et al., 2006; Wang et al., 2006, 2007).

5.3. GIS chronology

In this chapter we assess the chronology of GIS events and compare them to the NGRIP record (using the GICC05 timescale back to 60 ka BP and the GICC05modelext timescale for the earlier period - Johnsen et al., 2001; Svensson et al., 2008; Wolff et al., 2010).

We use the mid-point at transitions as the onset of climate events. The start of GIS 17 occurred at 59.4 ± 0.2 ka BP in the JFYK7 record, identical within error to stalagmites XY2 (59.5 ± 0.4 ka BP - Li et al., 2007) and MSL (59.7 ± 0.4 ka BP - Wang et al., 2001) and in agreement with the onset of GIS 17 in NGRIP (59.4 ± 2.6 ka BP - Capron et al., 2010).

There are some small discrepancies in the timing of GIS 18–20 events. Although they are within the 2σ counting error of the NGRIP time scale, it is worth examining them in more detail. The isotope maximum of GIS 18 occurred at 64.0 ± >2.6 ka BP in NGRIP and the GIS 18 isotope minimum is recorded at 64.6 ± 0.5 ka BP in XY2 (Fig. 5A and B). GIS 18 is not resolved in stalagmite SB22 from Sanbao Cave (Xia et al., 2007; Wang et al., 2008), but it is clearly registered in the Hulu Cave record at 64.4 ± 0.4 ka BP (Fig. 5C and D). The onset of GIS 19 occurred at 71.4 ± 0.3 ka BP in the JFYK7 stalagmite, compared to 72.3± >2.6 ka BP in NGRIP (Fig. 5A and B). Finally, the mid-points of the transitions into and out of GIS 20 are constrained to 74.8 ± 0.3 and 73.2 ± 0.3 ka BP in JFYK7, respectively, and to 76.4± >2.6 and 74.1± >2.6 ka BP in NGRIP (Fig. 5A and B).

The timing of GIS 18–20 is consistent among Chinese stalagmite records within age uncertainties (Fig. 5B–D). Assessing possible phase shifts between these and GIS events recorded in Greenland is presently difficult given the large age uncertainties (>2.6 ka) of the NGRIP chronology for MIS 4. The coherence of the timing of GIS 17 among various archives underscores the accuracy of the GICC05 timescale back to 60 ka BP. However, conspicuous discrepancies exist for GIS 18–20, suggesting that the accuracy of the Greenland ice-core chronology should be slightly revised for the section prior to 60 ka.

5.4. Heinrich 6

The chronology of H6 is still debatable, because its timing is beyond the limit of precise radiocarbon dating. Initially, the timing of H6 was defined at 65–66 ka BP (Heinrich, 1988; Bond et al., 1992). More recently, 60 ka BP has been considered to be a more acceptable age (Hemming, 2004). In the JFYK7 record, the isotope maximum corresponding to H6 is constrained by five ^{230}Th dates with uncertainties of less than 0.3‰ (Fig. 6C). The $\delta^{18}O$ values rapidly increase by 1.6‰ between 61.5 and 61.0 ka BP, indicating an abrupt weakening of the ASM (Fig. 6C). A similar isotope excursion is registered in the XY2 record, albeit with a lower amplitude (Fig. 6B). This abrupt transition is also seen in records from the Arabian Sea and the Cariaco Basin (Deplazes et al., 2013) (Fig. 6E and F). We regard the abrupt $\delta^{18}O$ increase in stalagmite JFYK7 as the onset of weak ASM conditions due to H6 and constrain the timing to 61.5 ± 0.2 ka BP. Given that there is no clear expression of H6 in the SB22 and MSL records (Figs. 5D and 6D), more high-resolution records are needed to confirm the proposed onset of H6 as identified in stalagmite JFYK7.

We define the mid-point of the transition from the isotopic maximum of H6 to GIS 17 as the end of H6, which is constrained to 59.4 ± 0.2 ka BP in JFYK7 and 59.5 ± 0.4 ka BP in XY2. This timing is in agreement with records – albeit of lower precision – from the Arabian Sea and the Cariaco Basin (Deplazes et al., 2013) (Fig. 6E and F). The H6 epoch constrained by the records from the mid to low latitudes of the NH does not correspond to the coldest period in Greenland, according to the NGRIP $\delta^{18}O$ record (Fig. 6A), but is consistent with the definition of the H6 between 60.1 and 63.2 ka BP, based on the NGRIP record (GICC05 chronology) (Sanchez and Harrison, 2010), which also is reflected by the Summit-NGRIP $\delta^{18}O$ difference anomalies (Seierstad et al., 2014).

It is well accepted that instabilities of the northern high latitude ice shelfs led to massive freshwater input into the North Atlantic during Heinrich events, which caused a strong reduction or even shutdown of the AMOC and consequent cooling in the North Atlantic realm (Heinrich, 1988; Hemming, 2004; McManus et al., 2004; Hodell et al., 2008). A close link between climate change over the northern high latitudes and ASM regions during Heinrich events has been previously suggested (Porter and An, 1995; Deplazes et al., 2014). For instance, the loess records from the Chinese Loess Plateau show that during the H6 event loess was deposited which is characterized by lower magnetic susceptibility values and larger grain sizes, indicating strong Asian winter monsoon and arid condition in northern China (Porter and An, 1995; Chen et al., 1997). The westerly winds have been proposed as the link between climate change in the North Atlantic realm and China during the last glacial period (Porter and An, 1995). More recently, Han et al. (2015) studied the succession of aeolian sand on the shore of Poyang Lake in South China and suggested that they were deposited during periods of weak EASM matching the Heinrich events (Han et al., 2015). In addition, Deplazes et al. (2014) studied the Indian summer monsoon variability using the elemental composition and grain size of a sediment core from the northeastern Arabian Sea. They found a strong reduction in precipitation in the Indus River catchment area and increased aridity on the Arabian Peninsula during H6, indicating a dramatically weakened ISM (Deplazes et al., 2014). These data in conjunction with our new JFYK7 record therefore suggest that the ASM regions, including South Asia, North and South China, experienced dry conditions during the H6 event. This can be explained partially by the cooling of the North Atlantic caused by massive iceberg discharges, which led to the southward migration of the mean position of ITCZ and subsequent weakening of the ASM (McManus et al., 2004; Zhang and Delworth, 2005; Deplazes et al., 2014).

5.5. GIS 18

Although JFYK7 did not record the abrupt strengthening of the ASM at the onset of GIS 18 because of a hiatus (Fig. 6C), stalagmite XY2, highly similar to JFYK7 during the overlapping interval, constrain the onset of GIS 18 to 64.7 ± 0.5 ka BP (Fig. 6B). GIS 18, originally recognized in the Greenland ice cores (Johnsen et al., 1992; Dansgaard et al., 1993), is also present in a number of other archives, including stalagmite MSL from Hulu cave (Wang et al.,

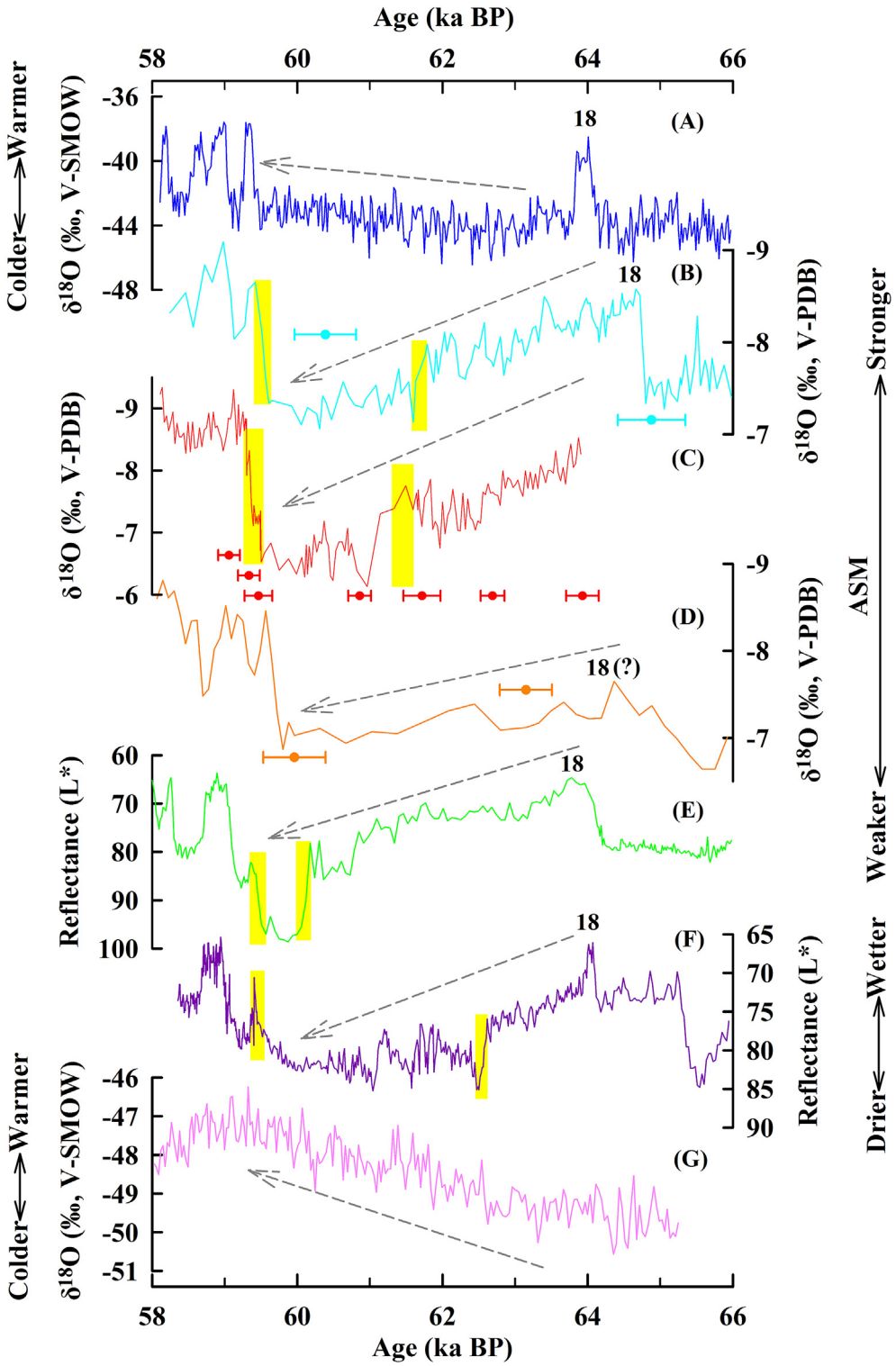

Fig. 6. Detailed comparison between JFYK7 and other records for the transition from GIS 18 to H6. (A) NGRIP (blue) (North Greenland Ice Core Project members, 2004). (B) Stalagmite XY2 (cyan) (Li et al., 2007). (C) Stalagmite JFYK7 (red). (D) Stalagmite MSL (orange) (Wang et al., 2001). (E) and (F) Total reflectance of sediments from the Arabian Sea (green) and the Cariaco Basin (purple) (100-points running mean) (Deplazes et al., 2013). (G) Antarctic EDML ice core (pink) (EPICA Community Members., 2006). ^{230}Th dates and associated uncertainties (±2σ) are shown for all stalagmite records. The yellow vertical bars mark the transitions into and out of the H6 event in each of the records. Based on the five high-precision ^{230}Th dates in the JFYK7 record the onset and end of H6 is constrained to 61.5 ± 0.2 and 59.4 ± 0.2 ka BP, respectively. The dashed gray lines with arrows denote the general trends leading from GIS 18 to H6. (For interpretation of the references to colour in this figure legend, the reader is referred to the web version of this article.)

2001), marine sediments from the Arabian Sea and the Cariaco Basin (Deplazes et al., 2013) and stalagmite BT2 from Brazil (Cruz et al., 2005) (Fig. 6A, D, 6E, 6F, 5F). Despite slight differences in the timing of GIS 18, its abrupt onset is obvious in records of sufficiently high resolution. However, the transition leading from GIS 18 to H6 is clearly different between NGRIP and records from the

mid to low NH latitudes (Fig. 6). In NGRIP, GIS 18 is characterized as an abrupt warming terminated by an equally rapid cooling (Fig. 6A). In contrast, the Chinese speleothem records suggest a gradual, millennial-scale decrease in the intensity of the ASM subsequent to GIS 18 (Fig. 6B). Additional records of high resolution are required to test this model of an abrupt onset and gradual end of GIS 18 in the ASM region. We note that a gradual transition from GIS 18 leading to H6 was also recorded in marine sediments from the Arabian Sea and the Cariaco Basin (Fig. 6C–F) (Deplazes et al., 2013).

During this gradual decline of the ASM (Fig. 6B–E) temperatures in Antarctica rose steadily (Fig. 6G) (EPICA Community Members., 2006). A similar situation occurred at the onset of H4, as shown by stalagmite records from central China (Zhou et al., 2014). We speculate that the discrepancy in the pattern of climate change between the ASM realm and Greenland can be attributed to changes of the transequatorial flow and the position of the ITCZ, both of which are linked to climate change in the SH. Modern meteorological research also demonstrates that the SH climate system, especially the Mascarene High and the transequatorial air flow, have a strong impact on the evolution of the ISM (Findlater, 1969; Krishnamurti and Bhalme, 1976; Wang and Xue, 2003) and the EASM (Gao et al., 2003; Sun et al., 2009). The temperature gradient between the SH and the NH is enhanced when the NH is colder/warmer and the SH is warmer/colder. As a result, the mean position of the ITCZ migrates towards the relatively warmer hemisphere (Chiang and Bitz, 2005; Broccoli et al., 2006; McGee et al., 2014). In addition, when the temperature of the SH decreases, both the Mascarene High and the transequatorial air flow, such as the Somali Jet, strengthen (An et al., 2000; 2011; Xue et al., 2004; Cai et al., 2006).

The temperature in Greenland dropped abruptly, i.e. within 120 yr, at ~64 ka BP at the end GIS 18 (Fig. 6A). At that time, the SH was still cold and the transequatorial flow was strong (Fig. 6G). Consequently, the mean position of the ITCZ failed to migrate southward following the cooling in the NH and the ASM did not weaken (Xue et al., 2004; Broccoli et al., 2006). Between 62.4 and 59.4 ka BP, the temperature in Greenland rose, but the amplitude was very small, remaining nearly in a stadial state (Fig. 6A). Meanwhile, Antarctica was warming strongly (Fig. 6G). As a result, the transequatorial flow became gradually weaker and the ITCZ migrated southward. This led to a gradual weakening of the ASM during the transition from GIS 18 to H6 rather than to an abrupt reduction.

6. Conclusions

The $\delta^{18}O$ record of stalagmite JFYK7, anchored by a more precise chronology and higher resolution than previous records from this region, provides a detailed picture of the centennial-to millennial-scale variability of the ASM during the period from 58.0 to 79.3 ka BP. The millennial-scale weak and strong ASM events correspond within dating uncertainties to H and GIS events, suggesting that the long-term evolution of the ASM was influenced by climate change in the NH high latitudes. The climate oscillations recorded by JFYK7 also have counterparts in other archives including Sanbao and Hulu Cave, the Arabian Sea, the Cariaco Basin and Brazil, suggesting a tight coupling on a global scale. The timing of CIS 17 in the JFYK7 record is consistent with that of GIS 17 in NGRIP, but minor differences exist between the two records with regard to the timing of GIS 18–20. Based on the precise ^{230}Th chronology with uncertainties of less than 0.3%, the onset and termination of H6 are constrained to 61.5 ± 0.2 and 59.4 ± 0.2 ka BP, respectively, in agreement with records from the mid- and low-latitudes of the NH. Compared to the rapid temperature drop in Greenland, the gradual decline of the ASM at the end of GIS 18 may have been influenced by the gradual warming in Antarctica.

Acknowledgements

This research was financially supported by the NSFC (Nos. 41172165, 41302138, and 41440020), "the Fundamental Research Funds for the Central Universities" (Nos. XDJK2013A012 and XDJK2014C010), "Karst Dynamics Laboratory, MLR and GZAR" (No. KDL201301) and the open project of "State Key Laboratory of Loess and Quaternary Geology" (No. SKLLQG1310) to T.-Y. Li and J.-Y. Li. This study was also supported by a Taiwan MOST grant (103-2119-M-002-022 to C.-C.S.).

References

Alley, R.B., 2005. Abrupt climate changes, oceans, ice, and us. Oceanography 17, 194–206.
An, Z.S., Clemens, S.C., Shen, J., Qiang, X.K., Jin, Z.D., Sun, Y.B., Prell, W.L., Luo, J.J., Wang, S.M., Xu, H., Cai, Y.J., Zhou, W.J., Liu, X.D., Liu, W.G., Shi, Z.G., Yan, L.B., Xiao, X.Y., Chang, H., Wu, F., Ai, L., Lu, F.Y., 2011. Glacial-interglacial Indian summer monsoon dynamics. Science 333, 719–723.
An, Z.S., Porter, S.C., Kutzbach, J.E., Wu, X.H., Wang, S.M., Liu, X.D., Li, X.Q., Zhou, W.J., 2000. Asynchronous holocene optimum of the East Asian monsoon. Quat. Sci. Rev. 19, 743–762.
An, Z.S., Wu, G.X., Li, J.P., Sun, Y.B., Liu, Y.M., Zhou, W.J., Cai, Y.J., Duan, A.M., Li, L., Mao, J.Y., Cheng, H., Shi, Z.G., Tan, L.C., Yan, H., Ao, H., Chang, H., Juan, F., 2015. Global monsoon dynamics and climate change. Annu. Rev. Earth Planet. Sci. 43, 29–77.
Barker, S., Knorr, G., 2007. Antarctic climate signature in the Greenland ice core record. Proc. Natl. Acad. Sci. U. S. A 104, 17278–17282.
Berger, A., Loutre, M.F., 1991. Insolation values for the climate of the last 10 million years. Quat. Sci. Rev. 10, 297–317.
Boch, R., Cheng, H., Spötl, C., Edwards, R.L., Wang, X., Häuselmann, P., 2011. NALPS: a precisely dated European climate record 120–60 ka. Clim. Past. 7, 1247–1259.
Bond, G., Broecker, W., Johnsen, S., McManus, J., Labeyrie, L., Jouzel, J., Bonani, G., 1993. Correlations between climate records from North Atlantic sediments and Greenland ice. Nature 365, 143–147.
Bond, G., Heinrich, H., Broecker, W., Labeyrie, L., McManus, J., Andrews, J., Huon, S., Jantschik, R., Clasen, S., Simet, C., Tedesco, K., Klas, M., Bonani, G., Ivy, S., 1992. Evidence for massive discharges of icebergs into the North Atlantic Ocean during the last glacial period. Nature 360, 245–249.
Broccoli, A.J., Dahl, K.A., Stouffer, R.J., 2006. Response of the ITCZ to northern hemisphere cooling. Geophys. Res. Lett. 33, L01702. http://dx.doi.org/10.1029/2005GL024546.
Broecker, W.S., 1998. Paleocean circulation during the last deglaciation: a bipolar seesea? Paleoceangraphy 13, 119–121.
Burns, S.J., Fleitmann, D., Matter, A., Kramers, J., Al-Subbary, A.A., 2003. Indian Ocean climate and an absolute chronology over Dansgaard/Oeschger events 9 to 13. Science 301, 1365–1367.
Cai, Y.J., An, Z.S., Cheng, H., Edwards, R.L., Kelly, M.J., Liu, W., Wang, X., Shen, C.C., 2006. High-resolution absolute-dated indian monsoon record between 53 and 36 ka from Xiaobailong cave, southwestern China. Geology 34, 621–624.
Cai, Y.J., Fung, I.Y., Edwards, R.L., An, Z.S., Cheng, H., Lee, J.E., Tan, L.C., Sheng, C.-C., Wang, X.F., Day, J.A., Zhou, W.J., Kelly, M.J., Chiang, J.C.H., 2015. Variability of stalagmite-inferred Indian monsoon precipitation over the past 252,000 y. Proc. Natl. Acad. Sci. U. S. A. 112, 2954–2959.
Caley, T., Roche, D.M., Renssen, H., 2014. Orbital Asian summer monsoon dynamics revealed using an isotope-enabled global climate model. Nat. Comm. 5, 5371. http://dx.doi.org/10.1038/ncomms6371.
Capron, E., Landais, A., Chappellaz, J., Schilt, A., Buiron, D., Dahl-Jensen, D., Johnsen, S.J., Jouzel, J., Lemieux-Dudon, B., Loulergue, L., Leuenberger, M., Masson-Delmotte, V., Meyer, H., Oerter, H., Stenni, B., 2010. Millennial and sub-millennial scale climatic variations recorded in polar ice cores over the last glacial period. Clim. Past. 6, 345–365.
Carolin, S.A., Cobb, K.M., Adkins, J.F., Clark, B., Conroy, J.L., Lejau, S., Malang, J., Tuen, A.A., 2013. Varied response of western Pacific hydrology to climate forcings over the last glacial period. Science 340, 1564–1566.
Chen, F.H., Bloemendal, J., Wang, J.M., Li, J.J., Oldfield, F., 1997. High-resolution multi-proxy climate records from Chinese loess: evidence for rapid climatic changes over the last 75 kyr. Palaeogeogr. Palaeoclimatol. Palaeoecol. 130, 323–335.
Cheng, H., Edwards, R.L., Shen, C.C., Polyak, V.J., Asmerom, Y., Woodhead, J., Hellstrom, J., Wang, Y., Kong, X., Spötl, C., 2013. Improvements in ^{230}Th dating, ^{230}Th and ^{234}U half-life values, and U-Th isotopic measurements by multi-collector inductively coupled plasma mass spectroscopy. Earth Planet. Sci. Lett. 371–372, 82–91.
Cheng, H., Edwards, R.L., Broecker, W.S., Denton, G.H., Kong, X., Wang, Y., Zhang, R., Wang, X., 2009. Ice age terminations. Science 326, 248–252.
Cheng, H., Sinha, A., Wang, X., Cruz, F.W., Edwards, R.L., 2012. The global Paleo-monsoon as seen through speleothem records from Asia and the Americas.

Clim. Dyn. 39, 1045–1062.
Chiang, J.C.H., Bitz, C.M., 2005. Influence of high latitude ice cover on the marine Intertropical Convergence Zone. Clim. Dyn. 25, 477–496.
Chiang, J.C.H., Biasutti, M., Battisti, D.S., 2003. Sensitivity of the Atlantic intertropical convergence zone to last glacial maximum boundary conditions. Paleoceanography 18, 1094. http://dx.doi.org/10.1029/2003PA000916.
Clement, A.C., Hall, A., Broccoli, A.J., 2004. The importance of precessional signals in the tropical climate. Clim. Dyn. 22, 327–341.
Cosford, J., Qing, H., Yuan, D.X., Zhang, M.L., Holmden, C., Patterson, W., Cheng, H., 2008. Millennial-scale variability in the Asian monsoon: evidence from oxygen isotope records from stalagmites in southeastern China. Palaeogeogr. Palaeoclimatol. Palaeoecol. 266, 3–12.
Cruz, F.W., Burns, S.J., Karmann, I., Sharp, W.D., Vuille, M., Cardoso, A.O., Ferrari, J.A., Silva Dias, P.L., Viana, O., 2005. Insolation-driven changes in atmospheric circulation over the past 116,000 years in subtropical Brazil. Nature 434, 63–66.
Dansgaard, W., Johnsen, S.J., Clausen, H.B., Clausen, H.B., Dahl-Jensen, D., Gundestrup, N.S., Hammer, C.U., Hvidberg, C.S., Steffensen, J.P., Sveinjörnsdottir, A.E., Jouzel, J., Bond, G., 1993. Evidence for general instability of past climate from a 250-kyr ice core record. Nature 364, 218–220.
Dayem, K.E., Molnar, P., Battisti, D.S., Roe, G.H., 2010. Lessons learned from oxygen isotopes in modern precipitation applied to interpretation of speleothem records of paleoclimate from eastern Asia. Earth Planet. Sci. Lett. 295, 219–230.
Deplazes, G., Lückge, A., Peterson, L.C., Timmermann, A., Hamann, Y., Hughen, K.A., Röhl, U., Laj, C., Cane, M.A., Sigman, D.M., Haug, G.H., 2013. Links between tropical rainfall and North Atlantic climate during the last glacial period. Nat. Geosci. 6, 213–217.
Deplazes, G., Lückge, A., Stuut, J.B.W., Pätzold, J., Kuhlmann, H., Husson, D., Fant, M., Haug, G.H., 2014. Weakening and strengthening of the Indian monsoon during Heinrich events and Dansgaard-Oeschger oscillations. Paleoceanography 29, 99–114.
Ding, Y.H., Chan, C.L., 2005. The East Asian summer monsoon: an overview. Meteorol. Atmos. Phys. 89, 117–142.
Ding, Y.H., Li, C.Y., Liu, Y.J., 2004. Overview of the south China sea monsoon experiment. Adv. Atmos. Sci. 2, 343–360.
Ding, Y.H., Wang, Z.Y., Sun, Y., 2008. Inter-decadal variation of the summer precipitation in East China and its association with decreasing Asian summer monsoon. Part I: observed evidences. Int. J. Climatol. 28, 1139–1161.
Ding, Z.L., Liu, T.S., Rutter, N.W., Yu, Z.W., Guo, Z.T., Zhu, R.X., 1995. Ice-volume forcing of East Asian winter monsoon variations in the past 800,000 years. Quat. Res. 44, 149–159.
Dorale, J.A., Liu, Z.H., 2009. Limitations of Hendy Test criteria in judging the paleoclimatic suitability of speleothems and the need for replication. J. Cave Karst Stud. 71, 73–80.
Drumond, A., Nieto, R., Gimeno, L., 2011. Sources of moisture for China and their variations during drier and wetter conditions in 2000–2004: a Lagrangian approach. Clim. Res. 50, 215–225.
Duan, F.C., Liu, D.B., Cheng, H., Wang, X.F., Wang, Y.J., Kong, X.G., Chen, S.T., 2014. A high-resolution monsoon record of millennial-scale oscillations during Late MIS 3 from Wulu Cave, south-west China. J. Quat. Sci. 29, 83–90.
Duan, F.C., Wu, J.Y., Wang, Y.J., Edwards, R.L., Cheng, H., Kong, X.G., Zhang, W.H., 2015. A 3000-yr annually laminated stalagmite record of the last glacial maximum from Hulu cave, China. Quat. Res. 83, 360–369.
EPICA Community Members, 2006. One-to-one coupling of glacial climate variability in Greenland and Antarctica. Nature 444, 195–198.
Fairchild, I.J., Smith, C.L., Baker, A., Fuller, L., Spötl, C., Mattey, D., McDermott, F., EIMF, 2006. Modification and preservation of environmental signals in speleothems. Earth-Sci. Rev. 75, 105–153.
Fleitmann, D., Burns, S.J., Mangini, A., Mudelsee, M., Kramers, J., Villa, I., Neff, U., Al-Subbary, A.A., Buettner, A., Hippler, D., 2007. Holocene ITCZ and Indian monsoon dynamics recorded in stalagmites from Oman and Yemen (Socotra). Quat. Sci. Rev. 26, 170–188.
Fleitmann, D., Burns, S.J., Mudelsee, M., Neff, U., Kramers, J., Mangini, A., Matter, A., 2003. Holocene forcing of the Indian monsoon recorded in a stalagmite from southern Oman. Science 300, 1737–1739.
Findlater, J., 1969. A major low-level air current near the Indian Ocean during the northern summer. Quart. J. R. Meteorol. Soc. 95, 362–380.
Gao, H., Xue, F., Wang, H.J., 2003. Influence of interannual variability of Antarctic oscillation on Mei-yu along the Yangtze and Huaihe River valley and its importance to prediction. Chin. Sci. Bull. 48, 61–67.
Han, L.Y., Li, T.Y., Cheng, H., Edwards, R.L., Shen, C.-C., Li, H.C., Huang, C.X., Li, J.Y., Yuan, N., Wang, H.B., Zhang, T.T., Zhao, X., 2016. Potential influence of temperature changes in the Southern Hemisphere on the evolution of the Asian summer monsoon during the last glacial period. Quat. Int. 392, 239–250.
Han, Z.Y., Li, X.S., Yi, S.W., Stevens, T., Chen, Y.Y., Wang, X.Y., Lu, H.Y., 2015. Extreme monsoon aridity episodes recorded in South China during Heinrich Events. Palaeogeogr. Palaeoclimatol. Palaeoecol. 440, 467–474.
Heinrich, H., 1988. Origin and consequences of cyclic ice rafting in the Northeast Atlantic Ocean during the past 130,000 years. Quat. Res. 29 (2), 142–152.
He, J.H., Zhao, P., Zhu, C.W., Zhang, R.H., Tang, X., Chen, L.X., Zhou, X.J., 2008. Discussion on the East Asian subtropical monsoon. Acta meteor. Sinica 66, 683–696.
Hemming, S.R., 2004. Heinrich events: massive late Pleistocene detritus layers of the North Atlantic and their global climate imprint. Rev. Geophys 42, RG1005. http://dx.doi.org/10.1029/2003 RG 000128.
Hendy, C.H., 1971. The isotopic geochemistry of speleothems-I. The calculation of the effects of different modes of formation on the isotopic composition of speleothems and their applicability as palaeoclimatic indicators. Geochim. Cosmochim. Acta 35, 801–824.
Hodell, D.A., Channell, J.E.T., Curtis, J.H., Romero, O.E., Röhl, U., 2008. Onset of "Hudson Strait" Heinrich events in the eastern North Atlantic at the end of the middle Pleistocene transition (similar to 640 ka)? Paleoceanography 23, PA4218. http://dx.doi.org/10.1029/2008PA001591.
Jaffey, A.H., Flynn, K.F., Glendenin, L.E., Bentley, W.C., Essling, A.M., 1971. Precision measurement of half-lives and specific activities of ^{235}U and ^{238}U. Phys. Rev. C4, 1889–1906.
Johnsen, S.J., Clausen, H.B., Dansgaard, W., Fuhrer, K., Gundestrup, N., Hammer, C.U., Iversen, P., Jouzel, J., Stauffer, B., Steffensen, J.P., 1992. Irregular glacial interstadials recorded in a new Greenland ice core. Nature 359, 311–313.
Johnsen, S.J., Dahl-Jensen, D., Gundestrup, N., Steffensen, J.P., Clausen, H.B., Miller, H., Masson-Delmotte, V., Sveinbjornsdottir, A.E., White, J., 2001. Oxygen isotope and palaeotemperature records from six Greenland ice-core stations: Camp Century, Dye-3, GRIP, GISP2, Renland and North GRIP. J. Quat. Sci. 16, 299–307.
Krishnamurti, T.N., Bhalme, H.N., 1976. Oscillation of a monsoon system, Part I: Observational aspects. J. Atmos. Sci. 33, 1937–1954.
Li, T.-Y., Shen, C.-C., Huang, L.-J., Jiang, X.-Y., Yang, X.-L., Mii, H.-S., Lee, S.-Y., Lo, L., 2014a. Stalagmite-inferred variability of the Asian summer monsoon during the penultimate glacial-interglacial period. Clim. Past. 10, 1211–1219.
Li, T.-Y., Shen, C.-C., Li, H.-C., Li, J.-Y., Chang, H.-W., Song, S.-R., Yuan, D.-X., Lin, C.D.J., Gao, P., Zhou, L.P., Wang, J.-L., Ye, M.-Y., Tang, L.-L., Xie, S.-Y., 2011. Oxygen and carbon isotopic systematics of aragonite speleothems and water in Furong Cave, Chongqing, China. Geochim. Cosmochim. Acta 75, 4140–4156.
Li, T.Y., Yuan, D.X., Li, H.C., Yang, Y., Wang, J.L., Wang, X.Y., Li, J.Y., Qin, J.M., Zhang, M.L., Lin, Y.S., 2007. High-resolution climate variability of southwest China during 57-70 ka reflected in a stalagmite δ^{18}O record from Xinya Cave. Sci. China Ser. D. 50, 1202–1208.
Li, Y., Wang, N.A., Zhou, X., Zhang, C., Wang, Y., 2014b. Synchronous or asynchronous Holocene Indian and East Asian summer monsoon evolution: a synthesis on Holocene Asian summer monsoon simulations, records and modern monsoon indices. Glob. Planet. Chang. 116, 30–40.
Liu, J.B., Chen, J.H., Zhang, X.J., Li, Y., Rao, Z.G., Chen, F.H., 2015. Holocene East Asian summer monsoon records in northern China and their inconsistency with Chinese stalagmite δ^{18}O records. Earth-Sci. Rev. 148, 194–208.
Liu, Y.H., Henderson, G.M., Hu, C.Y., Mason, A.J., Charnley, N., Johnson, K.R., Xie, S.C., 2013. Links between the East Asian monsoon and North Atlantic climate during the 8,200 year event. Nat. Geosci. 6, 117–120.
Liu, Z.Y., Wen, X.Y., Brady, E.C., Otto-Bliesner, B., Yu, G., Lu, H.Y., Cheng, H., Wang, Y.J., Zheng, W.P., Ding, Y.H., Edwards, R.L., Cheng, J., Liu, W., Yang, H., 2014. Chinese cave records and the East Asia summer monsoon. Quat. Sci. Rev. 83, 115–128.
McGee, D., Donohoe, A., Marshall, J., Ferreira, D., 2014. Changes in ITCZ location and cross-equatorial heat transport at the last glacial maximum, Heinrich stadial 1, and the mid-holocene. Earth Planet. Sci. Lett. 390, 69–79.
McManus, J.F., Francois, R., Gherardi, J.M., Keigwin, L.D., Brown-Leger, S., 2004. Collapse and rapid resumption of Atlantic meridional circulation linked to deglacial climate changes. Nature 428, 834–837.
Neff, U., Burns, S.J., Mangini, A., Mudelsee, M., Fleitmann, D., Matter, A., 2001. Strong coherence between solar variability and the monsoon in Oman between 9 and 6 kyr ago. Nature 411, 290–293.
Ninkovich, D., Shackleton, N.J., Abdel-Monem, A.A., Obradovich, J.D., Izett, G., 1978. K-Ar age of the late Pleistocene eruption of Toba, north Sumatra. Nature 276, 574–577.
North Greenland Ice Core Project members, 2004. High-resolution record of Northern Hemisphere climate extending into the last interglacial period. Nature 431, 147–151.
O'Neil, J.R., Clayton, R.N., Mayeda, T.K., 1969. Oxygen isotope fractionation in divalent metal carbonates. J. Chem. Phys. 51, 5547–5559.
Pausata, F.S., Battisti, D.S., Nisancioglu, K.H., Bitz, C.M., 2011. Chinese stalagmite δ^{18}O controlled by changes in the Indian monsoon during a simulated Heinrich event. Nat. Geosci. 4, 474–480.
Porter, S.C., An, Z.S., 1995. Correlation between climate events in the North Atlantic and China during the last glaciation. Nature 375, 305–308.
Rampino, M.R., Self, S., 1992. Volcanic winter and accelerated glaciation following the Toba super-eruption. Nature 359, 50–52.
Rampino, M.R., Self, S., 1993. Climate-volcanism feedback and the Toba eruption of ~74 000 years ago. Quat. Res. 40, 269–280.
Robock, A., Ammann, C.M., Oman, L., Shindell, D., Levis, S., Stenchikov, G., 2009. Did the Toba volcanic eruption of ~74 ka B.P. produce widespread glaciation? J. Geophys. Res. 114, D10107. http://dx.doi.org/10.1029/2008JD011652.
Rohling, E.J., Liu, Q.S., Roberts, A.P., Stanford, J.D., Rasmussen, S.O., Langen, P.L., Siddall, M., 2009. Controls on the East Asian monsoon during the last glacial cycle, based on comparison between Hulu Cave and polar ice-core records. Quat. Sci. Rev. 28, 3291–3302.
Sagawa, T., Kuwae, M., Tsuruoka, K., et al., 2014. Solar forcing of centennial-scale East Asian winter monsoon variability in the mid to late Holocene. Earth Planet. Sci. Lett. 395, 124–135.
Sanchez Goñi, M.F., Harrison, S.P., 2010. Millennial-scale climate variability and vegetation changes during the Last Glacial: concepts and terminology. Quat. Sci. Rev. 29, 2823–2827.
Scholz, D., Hoffmann, D.L., 2011. StalAge - an algorithm designed for construction of speleothem age models. Quat. Geochronol. 6, 369–382.

Schulz, H., Emeis, K.C., Erlenkeuser, H., von Rad, U., Rolf, C., 2002. The Toba volcanic event and interstadial/stadial climates at the Marine Isotopic Stage 5 to 4 transition in the northern Indian Ocean. Quat. Res. 57, 22–31.
Seierstad, I.K., Abbott, P.M., Bigler, M., Blunier, T., Bourne, A.J., Brook, E., Buchardt, S.L., Buizert, C., Clausen, H.B., Cook, E., Dahl-Jensen, D., Davies, S.M., Guillevic, M., Johnsen, S.J., Pedersen, D.S., Popp, T.J., Rasmussen, S.O., Severinghaus, J.P., Svensson, A., Vinther, B.M., 2014. Consistently dated records from the Greenland GRIP, GISP2 and NGRIP ice cores for the past 104 ka reveal regional millennial-scale $\delta^{18}O$ gradients with possible Heinrich event imprint. Quat. Sci. Rev. 106, 29–46.
Self, S., 2006. The effects and consequences of very large explosive volcanic eruptions. Philos. T. R. Soc. A 364, 2073–2097.
Shakun, J.D., Burns, S.J., Fleitmann, D., Kramers, J., Matter, A., Al-Subary, A., 2007. A high-resolution, absolute-dated deglacial speleothem record of Indian Ocean climate from Socotra Island, Yemen. Earth Planet. Sci. Lett. 259, 442–456.
Shen, C.-C., Cheng, H., Edwards, R.L., Moran, S.B., Edmonds, H.N., Hoff, J.A., Thomas, R.B., 2003. Measurement of attogram quantities of ^{231}Pa in dissolved and particulate fractions of seawater by isotope dilution thermal ionization mass spectroscopy. Anal. Chem. 75, 1075–1079.
Shen, C.-C., Wu, C.-C., Cheng, H., Edwards, R.L., Hsieh, Y.-T., Gallet, S., Chang, C.-C., Li, T.-Y., Lam, D.D., Kano, A., Hori, M., Spötl, C., 2012. U-Th isotopic determinations in femtogram quantities and high-precision and high-resolution carbonate ^{230}Th dating by MC-ICP-MS with SEM protocols. Geochim. Cosmochim. Acta 99, 71–86.
Sinha, A., Cannariato, K.G., Stott, L.D., Li, H.C., You, C.F., Cheng, H., Edwards, R., Singh, I.B., 2005. Variability of Southwest Indian summer monsoon precipitation during the Bølling–Allerød. Geology 33, 813–816.
Sirocko, F., 2003. What drove past teleconnections? Science 301, 1336–1337.
Steinke, S., Glatz, C., Mohtadi, M., Groeneveld, J., Li, Q., Jian, Z., 2011. Past dynamics of the East Asian monsoon: no inverse behaviour between the summer and winter monsoon during the Holocene. Glob. Planet. Change 78, 170–177.
Storey, M., Roberts, R.G., Saidin, M., 2012. Astronomically calibrated $^{40}Ar/^{39}Ar$ age for the Toba supereruption and global synchronization of late Quaternary records. Proc. Natl. Acad. Sci. U. S. A. 109, 18684–18688.
Stríkis, N.M., Chiessi, C.M., Cruz, F.W., Vuille, M., Cheng, H., de Souza Barreto, E.A., Mollenhauer, G., Kasten, S., Karmann, I., Edwards, R.L., Bernal, J.P., dos Reis Sales, H., 2015. Timing and structure of Mega-SACZ events during Heinrich Stadial 1. Geophys. Res. Lett. 42, 5477–5484.
Sun, J.Q., Wang, H.J., Yuan, W., 2009. A possible mechanism for the co-variability of the boreal spring Antarctic Oscillation and the Yangtze River valley summer rainfall. Int. J. Clim. 29, 1276–1284.
Sun, Y.B., Clemens, S.C., Morrill, C., Lin, X.P., Wang, X.L., An, Z.S., 2012. Influence of Atlantic meridional overturning circulation on the East Asian winter monsoon. Nat. Geosci. 5, 46–49.
Svensson, A., Andersen, K.K., Bigler, M., Clausen, H.B., Dahl-Jensen, D., Davies, S.M., Johnsen, S.J., Muscheler, R., Parrenin, F., Rasmussen, S.O., Röthlisberger, R., Seierstad, I., Steffensen, J.P., Vinther, B.M., 2008. A 60,000 year Greenland stratigraphic ice core chronology. Clim. Past. 4, 47–57.
Tan, M., 2009. Circulation effect: Climatic significance of the short term variability of the oxygen isotopes in stalagmites from monsoonal China—Dialogue between paleoclimate records and modern climate research. Quat. Sci. 29, 851–862 (in Chinese, with English abstract).
Tan, M., 2011. Tread-wind driven inverse coupling between stalagmite δ18O from monsoon region of China and large scale temperature—circulation effect on decadal to precessional timescales. Quat. Sci. 31, 1086–1097 (in Chinese, with English abstract).
Tan, M., 2014. Circulation effect: response of precipitation $\delta^{18}O$ to the ENSO cycle in monsoon regions of China. Clim. Dyn. 42, 1067–1077.
Tao, S., Chen, L., 1987. A review of recent research on the East Asian summer-monsoon. In: Chang, C.-P., Krishnamurti, T.N. (Eds.), China, Monsoon Meteorology. Oxford University Press, London, pp. 60–92.
Taylor, S.R., McLennan, S.M., 1995. The geochemical evolution of the continental crust. Rev. Geophys. 33, 241–265.
Tian, H., Guo, P.W., Lu, W.S., 2004. Characteristics of vapor inflow corridors related to summer rainfall in China and impact factors. J. Trop. Meteorol. 20, 401–408.
Timmreck, C., Graf, H.F., Zanchettin, D., Hagemann, S., Kleinen, T., Krüger, K., 2012. Climate response to the Toba super-eruption: Regional changes. Quat. Int. 258, 30–44.
Waelbroeck, C., Labeyrie, L., Michel, E., Duplessy, J.C., McManus, J.F., Lambeck, K., Balbon, E., Labracherie, M., 2002. Sea-level and deep water temperature changes derived from benthonic foraminifera isotopic records. Quat. Sci. Rev. 21, 295–305.
Wang, B., Lin, H., 2002. Rainy season of the Asian-Pacific summer monsoon. J. Clim. 15, 386–396.
Wang, H.B., Li, T.Y., Yuan, N., Li, J.Y., 2014a. Environmental signification and the characteristics of δD and $\delta^{18}O$ variation in the local precipitation and drip water in Yangkou cave. Chongqing. Carsologica Sin. 33, 146–155 (in Chinese, with English abstract).
Wang, H.J., Chen, H.P., 2012. Climate control for southeastern China moisture and precipitation: Indian or East Asian monsoon? J. Geophys. Res. 117, D12109. http://dx.doi.org/10.1029/2012JD017734.
Wang, H.J., Xue, F., 2003. The interannual variability of Somali jet and its influences on the inter-hemispheric water vapor transport and the East Asian summer rainfall. Chin. J. Geophys. 46, 11–20.
Wang, P.X., Wang, B., Cheng, H., Fasullo, J., Guo, Z.T., Kiefer, T., Liu, Z.Y., 2014b. The global monsoon across timescales: coherent variability of regional monsoons. Clim. Past. 10, 2007–2052.
Wang, X.F., Auler, A.S., Edwards, R.L., Cheng, H., Ito, E., Solheid, M., 2006. Interhemispheric anti-phasing of rainfall during the last glacial period. Quat. Sci. Rev. 25, 3391–3403.
Wang, X.F., Auler, A.S., Edwards, R.L., Cheng, H., Ito, E., Wang, Y.J., Kong, X.G., Solheid, M., 2007. Millennial-scale precipitation changes in southern Brazil over the past 90,000 years. Geophys. Res. Lett. 34, L23701. http://dx.doi.org/10.1029/2007GL031149.
Wang, Y.J., Cheng, H., Edwards, R.L., An, Z.S., Wu, J.Y., Shen, C.-C., Dorale, J.A., 2001. A high resolution absolute-dated Late Pleistocene monsoon record from Hulu Cave, China. Science 294, 2345–2348.
Wang, Y.J., Cheng, H., Edwards, R.L., He, Y., Kong, X., An, Z.S., Wu, J.Y., Kelly, M.J., Dykoski, C.A., Li, X., 2005. The Holocene Asian monsoon: links to solar changes and North Atlantic climate. Science 308, 854–857.
Wang, Y.J., Cheng, H., Edwards, R.L., Kong, X.G., Shao, X.H., Chen, S.T., Wu, J.Y., Jiang, X.Y., Wang, X.F., An, Z.S., 2008. Millennial- and orbital-scale changes in the East Asian monsoon over the past 224,000 years. Nature 451, 1090–1093.
Williams, M.A.J., Ambrose, S.H., van der Kaars, S., Ruehlemann, C., Chattopadhyaya, U., Pal, J., Chauhan, P.R., 2009. Environmental impact of the 73 ka Toba supereruption in South Asia. Palaeogeogr. Palaeoclimatol. Palaeoecol. 284, 295–314.
Wolff, E.W., Chappellaz, J., Blunier, T., Rasmussen, S.O., Svensson, A., 2010. Millennial-scale variability during the last glacial: The ice core record. Quat. Sci. Rev. 29, 2828–2838.
Xia, Z.F., Kong, X.G., Jiang, X.Y., Cheng, H., 2007. Precise dating of East-Asian-Monsoon D/O events during 95-56 ka BP: Based on stalagmite data from Shanbao Cave at Shennongjia. China. Sci. China Ser. D. 50, 228–235.
Xue, F., Wang, H., He, J., 2004. Interannual variability of Mascarene High and Australian High and their influences on East Asian summer monsoon. J. Meteorol. Soc. Jpn. 82, 1173–1186.
Yuan, D.X., Cheng, H., Edwards, R.L., Dykoski, C.A., Kelly, M.J., Zhang, M.L., Qing, J.M., Lin, Y.S., Wang, Y.J., Wu, J.Y., Dorale, J.A., An, Z.S., Cai, Y.J., 2004. Timing, duration, and transitions of the Last Interglacial Asian monsoon. Science 304, 575–578.
Zhang, D.E., Lu, L.H., 2007. Anti-correlation of summer/winter monsoons? Nature 450, E7–E8.
Zhang, R., Delworth, T.L., 2005. Simulated tropical response to a substantial weakening of the Atlantic thermohaline circulation. J. Clim. 18, 1853–1860.
Zhang, R., Zhu, X.W., Han, D.S., Zhang, Y.H., Fang, F.B., 1998. Preliminary study on karst caves of MT. Jinfo, Nanchuan, Chongqing. Carsologica Sin. 17, 196–211 (in Chinese, with English abstract).
Zhao, P., Zhou, X.J., 2006. Decadal variability of rainfall persistence time and rainbelt shift over Eastern China in recent 40 years. Q. J. Appl. Meteorol. 17, 548–556 (in Chinese, with English abstract).
Zhou, H.Y., Zhao, J.X., Feng, Y.X., Chen, Q., Mi, X.J., Shen, C.C., He, H.B., Yang, L., Liu, S.H., Chen, L., Huang, J.Y., Zhu, L.Y., 2014. Heinrich event 4 and Dansgaard/Oeschger events 5-10 recorded by high-resolution speleothem oxygen isotope data from central China. Quat. Res. 82, 394–404.
Zielinski, G.A., Mayewski, P.A., Meeker, L.D., Whitlow, S., Twickler, M.S., 1996. Potential atmospheric impact of the Toba mega-eruption ~71,000 years ago. Geophys. Res. Lett. 23, 837–840.